J. Inst. Eng. India Ser. C (February 2022) 103(1):121–133
https://doi.org/10.1007/s40032-021-00728-1

REVIEW PAPER

The Small Punch Test a Viable Alternate for In-service Components Preserved Strength Estimation

Pruthvish Patel[1] · **B. K. Patel**[2]

Received: 10 January 2021 / Accepted: 7 June 2021 / Published online: 13 July 2021

Abstract The small punch test (SPT) is a miniature specimen testing technique to extract the mechanical strength characterization of the in-service component—to determine its preserved strength and fitness-for-service. This technique delivers a convincing test outcome inline to conventional testing using a universal testing machine. The bulk material to retrieve from the in-service component for testing is quite challenging without compromising the structural strength integrity so this technique comes in handy to serve the purpose. During the SP testing, the miniaturized specimen is indented using a rigid ball punch, and the specimen's load–displacement response is measured simultaneously. Such load–displacement response is post-processed further to determine the preserved strength parameters to assess the remaining life of the system to be fit for service. During the last couple of decades, numerous research advancements are made and several researchers have proposed various graphical and analytical approaches to improve the strength determination and mechanical characterization practice. However, many diverse opinions emerged in the efforts to formulate the reliable and universal mechanical characterization approach, using the SPT load–displacement data. This paper attempts to summarize the latest developments which are made and verifying the viability of popular graphical and analytical approaches for non-irradiated ductile iron, 65-45-12 material which is extracted from the in-service general-purpose mechanical system. It is also outlined the certain challenges and potential scope of improvement for SPT technique.

Keywords SPT · Small punch test · Fitness-for-service · Miniature testing · Specimen test · Tensile strength

Introduction

The small punch test (SPT) is an evolving miniature specimen test technique that was developed in the late 1980s by many researchers [1–4]. This technique is highly effective to determine the preserved structural strength integrity and residual life [5] of the in-service component to realize its fitness-for-service. This approach was primarily explored over irradiated and embrittled specimens retrieved from the nuclear and steam power plants [2, 4, 6, 7] for the subjected purpose but later, its novelty was expanded further for general engineering system applications [8–10].

The credible attempts have been made to establish the reliable and universally viable correlations and methodologies—to determine the mechanical strengths from the SPT load–displacement response. The objective of this paper is to narrate the recent development, those are made toward estimation of in-service component's structural strength integrity. It is also verified the viability of popular graphical and empirical correlations for the ductile iron, 65-45-12 material's characterization which is extracted from one of the general-purpose mechanical systems.

✉ Pruthvish Patel
prithvish.patel@gmail.com

[1] Gujarat Technological University, Ahmedabad, Gujarat, India

[2] Mechanical Engineering Department, L. D. College of Engineering, Ahmedabad, Gujarat, India

Small Punch Test

The small punch test was first developed at MIT for radiation embrittlement studies and reported by Manahan et al. [1], and further research was extended by Mao et al. [11]. The SP test apparatus includes a miniature specimen, the lower and upper dies, spherical tipped punch, or spherical ball punch separately. As shown in Fig. 1, the specimen is clamped firmly in-between the dies whereas the specimen is indented using the spherical punch at a gradual force.

Where (1) specimen (2) spherical tipped punch (3) lower die (4) upper die (5) deflection measurement rod. d_1 = 8 mm, d_2 = 4 mm, r = 1.25 mm, u_1 = punch displacement, u_2 = specimen displacement, t_0 = initial specimen thickness, P = applied load.

It is recommended to have a punch hardness of at least 55 HRC for steel specimens to ensure that it doesn't deform during the punching. Traditionally, the flat circular or square-shaped, 0.2–0.5 mm thick miniature specimens are utilized [11, 12] for SPT; excluding Simonovski et al. [8] researched over the curved specimens.

The initial attempt had been made at Japanese Atomic Energy Research Institute (JAERI) by Takahashi et al. [13] to standardize the SP test practice for metallic materials to determine the ductile to brittle transition temperature (DBTT) and elastic–plastic fracture toughness (J_{IC}). Later, European committee of standardization (CEN) [5] worked to standardize the SP test a code of practice for tensile and fracture behavior for metallic material, where they referred to the indenter load as a function of the diameter of indenting ball, specimen thickness and lower die diameter.

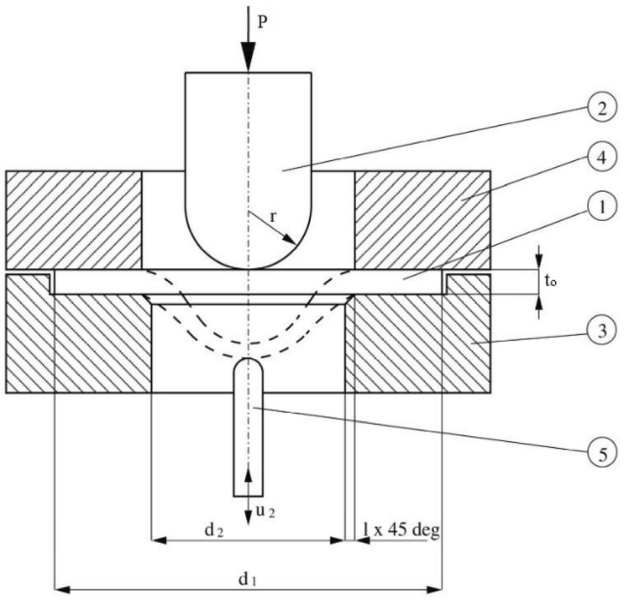

Fig. 1 Schematic representation of the SPT testing device [5].

Such SPT setup is attached to the universal testing machine equipped with a load cell of 5–20 kN. Generally, the indentation is carried out at the very slower displacement rate of 0.2 mm/min until the specimen ruptures and corresponding specimen displacement is measured using a precise extensometer [8, 14, 15]. As an SP test output, the load–displacement characteristic curve is generated.

The miniature specimens are being developed using either virgin or aged material under investigation. Manahan et al. [1] stamped the specimens from rolled sheets and Mao et al. [11], sliced from steel rod of ø3.0 mm to define the SPT technique. Generally, the aged material specimens are scooped out using the sampler machines as shown in Figs. 2, 3a, whereby surface material is removed through a mechanically powered cutting mechanism. Later, the extracted material is shaped into miniature specimen blanks as Fig. 3b, employing EDM cutting, followed by polishing to make them SP test compliant. Such scooping techniques, minimally invade the in-service component, as a result, its structural integrity remains intact.

Since the computer-added finite element analysis (FEA) simulation tool capabilities have been advanced, researchers [1, 8, 18, 19] have adopted the FE simulation-driven approach to research the insight of specimens characteristic transformation under the instantaneous loading. Many times, it is also preferred to simulate the SP test virtually, rather than to conduct experimental testing. First-ever Manahan et al. [1], explored the potential of FEA to convert the experimentally measured load–deflection data into stress/strain information. Numerical simulation has been performed using implicit non-linear solver by resembling the real SP test boundary conditions as shown in Fig. 4. The FEA geometry is typically idealized by 2D axisymmetric elements to optimize the result accuracy and computation time over the use of 3D elements due to reduced order degrees of freedom and highly mapped mesh control. Axisymmetric 2D elements are featured to globalize the elemental stiffness behavior across the stipulated angle with reference of datum axis. These elements are equally capable to deliver reliable results using 3D elements. The frictionless contacts are defined between punch-upper die whereas the specimen is tightly clamped in-between the upper and lower dies. The free surfaces of upper-lower dies are constrained as fixed. The SPT specimen is defined using isotropic elastic–plastic non-linear material characteristics.

All the components except the specimen are considered as a rigid to eliminate the simulation compliance error. The punch follows the 2–3 mm of displacement load and indenting the specimen under the frictional/frictionless environment until it ruptures. The frictionless condition imitates the SP testing over the lubricated specimen,

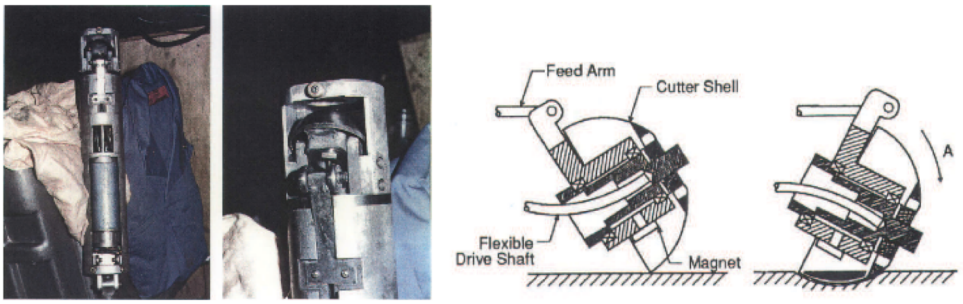

Fig. 2 Abrasive-edged spinning cutter shell [16]

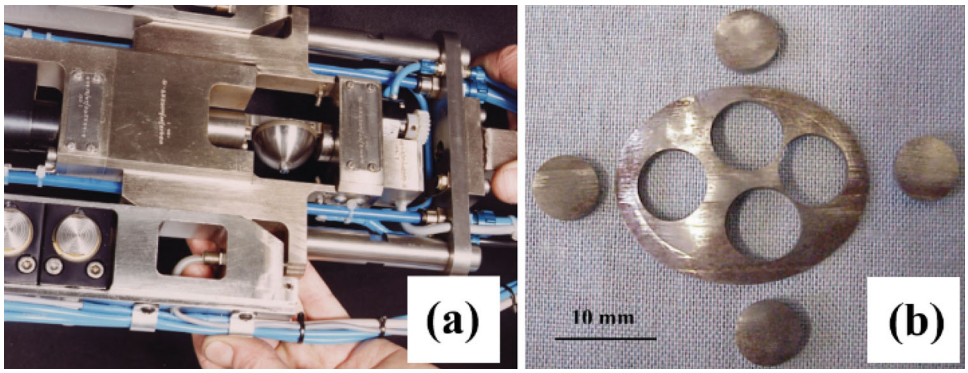

Fig. 3 **a** Nuclear reactor pressure vessel sampler [17], **b** Specimen blanks machined using EDM out of sample removed with the scoop system [5]

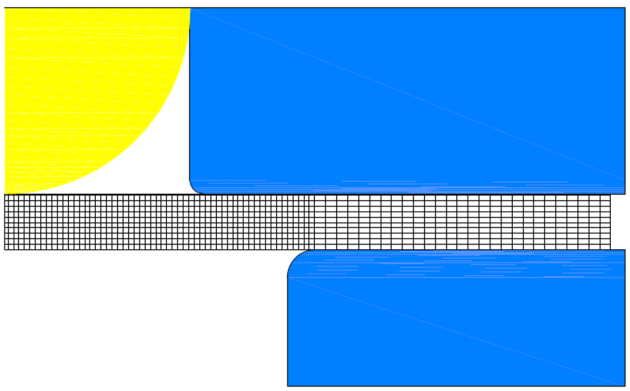

Fig. 4 Axisymmetric numerical model setup

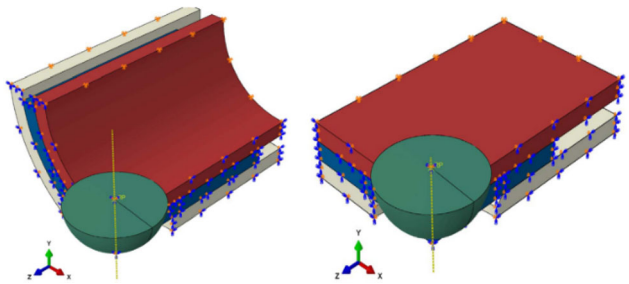

Fig. 5 1/4 symmetric FE model of flat and curved specimens [8]

whenever the study is not meant to verify the friction sensitivity.

Simonovski et al. [8] has conducted an SP test over the flat and curved specimens to verify the specimen's geometrical stiffness sensitivity for mechanical characterization. Later the experimental results were compared through FE models as shown in Fig. 5.

Load–Displacement (L–D) Curve

During SP testing, the specimen deforms under the indented load. Such constitutive relations are outlined in form of L–D curve. The Manahan et al. [1] represented the L–D curve at room temperature for the 316SS with 20% cold work material as shown in Fig. 6 and similarly, Mao et al. [11] performed the SP test using various grades of steel material and varied L–D responses are plotted in Fig. 7. Such variation is primarily realized due to variation in material's inherent elastic–plastic stiffnesses and fracture toughness. Fleury et al. [20] performed the SP testing for the temperature range of 25–600 °C and noticed that maximum load is decreasing with elevated temperature as shown in Fig. 8. Such a trend of observation conforms the metal's uniaxial strength deterioration along with temperature increment.

Figure 9 defines the classical form of metallic specimens' L–D characteristic curve. The specimen displacement behavior has been classified into four zones by Kameda et al. [21]. I-Elastic bending of the specimen due to contact with indenter, II-Plastic bending due to continuous deflection, III-Plastic membrane stretching happens after reaching certain plastic bending limit and IV-Plastic instability where necking and specimen cracking starts after reaching maximum load whereas fracture is happening in different regime with reference of its fracture

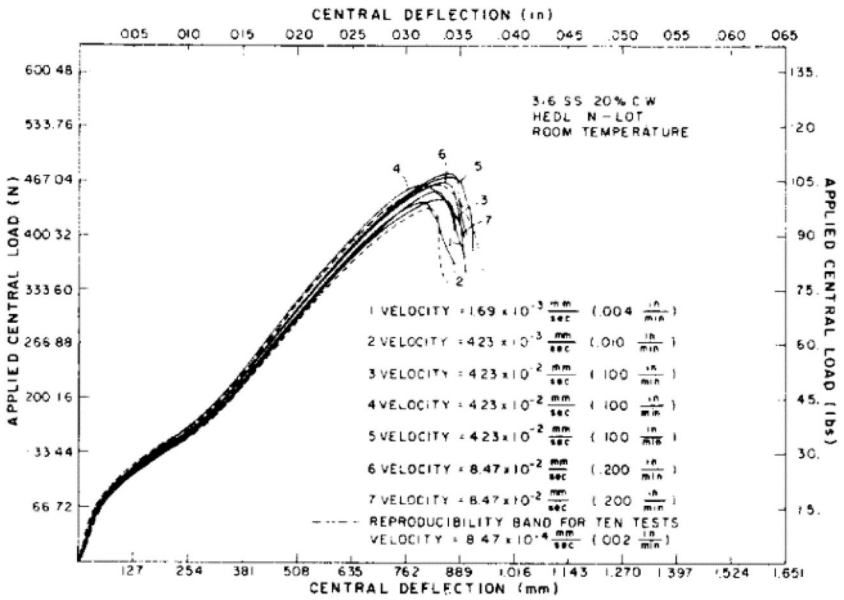

Fig. 6 L–D curve 316SS with 20% cold work [1]

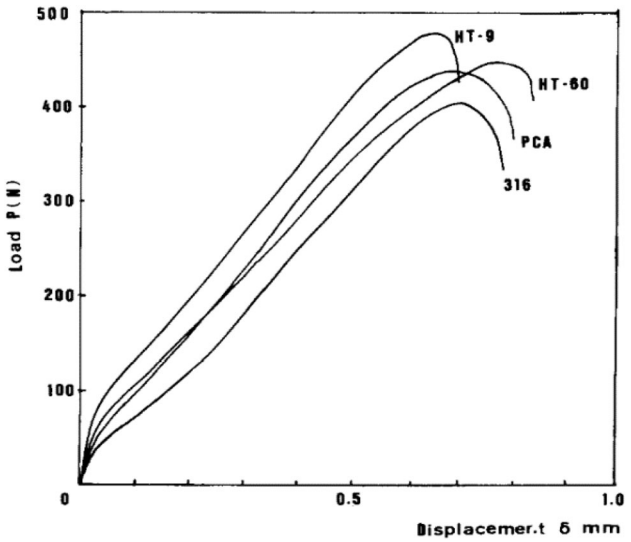

Fig. 7 L–D curve of various metal specimens at room temperature [11]

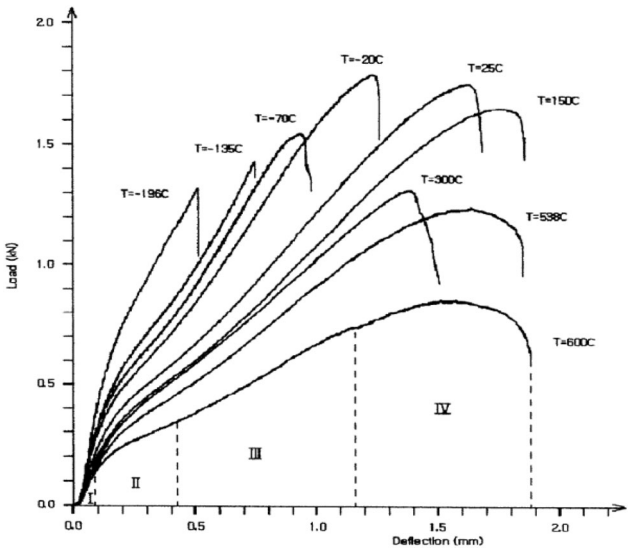

Fig. 8 Load–displacement curve for 12Cr–1Mo [20]

toughness—is not defined here. This L–D behavior is characterized using Eqs. (1) to (4).

Pilkey [22] in the book "Formula for stress, strain, and structural matrices" has proposed the equations to model the elastic bending behavior. The elastic deflection has been determined as a function of applied load through Eq. (1).

$$P = \frac{64I\delta_e\left[1-\left(1-\delta_e^2\right)\right]^{1/2}}{1.504(d/2)^2(L/2)^4[C_1+2C_2(1-\alpha^2)+\alpha^2]} \quad (1)$$

where C_1, C_2 and α = the geometrical constants, d = indenter diameter, P = applied load, δ_e = elastic deflection, and I = moment of inertia.

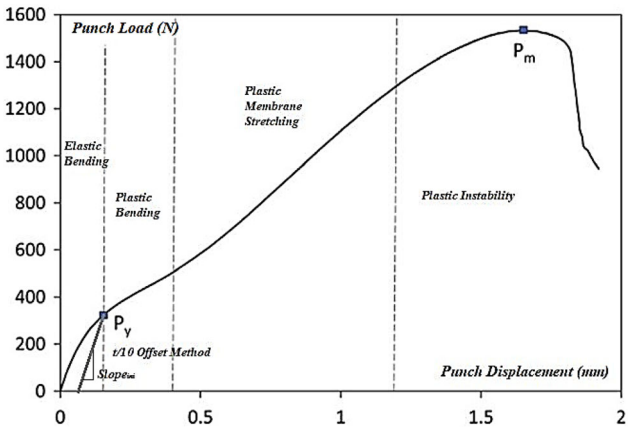

Fig. 9 Metals load–displacement curve at room temperature

Whereas, plastic bending behavior is described by Drucker–Prager constitutive equation [23] with the assumption of all the SPT components are perfectly rigid except miniature specimen. He defined to calculate the plastic stress and strain using Eqs. (2) and (3), respectively.

$$\sigma = \frac{CP_e}{4\pi\left[0.721(Pd\gamma)^{0.33}\right](t_0/3)} \tag{2}$$

where C = constant for the distributed load, P_e = load determined from the elastic calculation, P = applied load, d = indenter diameter, γ = Poisson's ratio, and t_0 = initial specimen thickness

$$\dot{\varepsilon}_p = K\left(\frac{\sigma}{\sigma_y} - 1\right)^n \tag{3}$$

where σ = plastic stress from Eq. (2), σ_y = yield stress, K and n = strain hardening constants determined from uniaxial tensile test data.

Zone III, Plastic membrane stretching behavior is explained by Wang [24] using Hill's plasticity theory based on a stress–strain incremental equation. The strains across the thickness,ε_t can be determined using fundamental Eq. (4).

$$\varepsilon_t = \ln\left(\frac{t}{t_0}\right) \tag{4}$$

where t = deformed thickness, and t_0 = initial specimen thickness

Fleury et al. [20] have verified the validity of Eqs. (1)–(4), by performing an SP test using austenitic 12Cr-1Mo and 1Cr-0.5Mo steels specimens along with temperature variation. Figure 10 shows the comparative data at 25 °C. The analytical simulation data found good alignment with the experimental data for elastic bending, plastic bending, and membrane stretching regimes.

Tensile Material Properties

Determination of yield force P_y and ultimate strength σ_u

Lucas et al. [25] experimentally investigated the effects of indenter ball size and specimen thickness on the SPT L–D response. The authors observed that:

1. Increasing specimen thickness; increases the yield load, maximum load, and displacement to rupture, due to gain in the bending stiffness.
2. The yield and maximum load increase with increment of punch ball size whereas displacement to rupture decreases slightly.

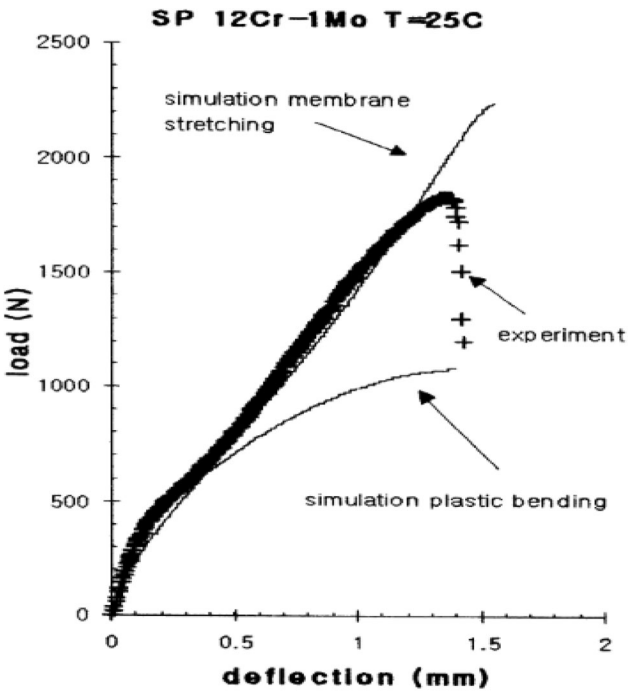

Fig. 10 Simulation of the SP plastic bending and membrane stretching regime at 25 °C [20]

It is extensively researched for SP tests using the various grades of austenitic and ferritic steels to establish the empirical correlations to estimate the yield stress, σ_y and the ultimate stress, σ_u. There is consensus found among the researchers for the potential use of linear equations such as Eqs. (5) to (7) for mechanical strength determination. These linear correlations are established by the normalization of P_y with t_0^2 Eq. (5) and P_m with t_0^2, $t_0\delta_m$ [i.e., Eqs. (6) and (7)].

$$\sigma_y = \alpha_1 + \frac{\alpha_2 P_y}{t_0^2} \tag{5}$$

$$\sigma_u = \beta_1 + \frac{\beta_2 P_m}{t_0^2} \tag{6}$$

$$\sigma_u = \beta_1' + \frac{\beta_2' P_m}{t_0 \delta_m} \tag{7}$$

, where t_0 = specimen initial thickness, P_m = maximum load in a load–displacement curve, P_y = elastic plastic transition force, and δ_m = deflection at maximum force. The correlation factors $\alpha_i, \beta_i, \beta_i'$ depend on the dimensions of the test rig such as punch diameter or diameter of the lower die.

However, the correlation factor values are significantly scattering to correlate the linear equations with graphical methods to characterize the various class of materials. Some researchers outlined the linear correlations with [26] or without [11] integration of the correlation factors $\alpha_2, \beta_2, \beta_2'$. The published distinct linear correlations along

with the corresponding factors with reference of boundary conditions are listed in Table 1.

Apart from the empirical formulations, many researchers [14, 15, 26, 35] explored the viability of various graphical methods for stress estimations. The widely reliable graphical methods include the offset method, CWA, and the two-tangent method. The offset method approach is similar to $R_{p0.2}$ strain offset method which is being

Table 1 Constants values for the SPT load–displacement correlations to determine the yield and ultimate strengths

Sr. no.	Reference	Material, temperature	Method	α_1	α_2	β_1	β_2	β'_1	β'_2
1	Mao and Takahashi [11]	Austenitic and ferritic steels, [25 °C]	2-Tangent	0	0.36	−320	0.13	–	–
2	Kameda and Mao [21]	Various austenitic and ferritic steels, [− 196 °C, 200 °C]	2-Tangent	0	0.36	–	–	–	–
3	Fleury and Ha [20]	4 different austenitic and ferritic steels [25 °C, 600 °C]	Not specified	0	0.33	–	–	–	–
4	Ruan et al. [27]	EUOFER97, [− 193 °C, 20 °C]	2-Tangent	149 ± 108	0.345–0.481	218 ± 101	0.062–0.092	–	–
5	Campitelli et al. [28]	316L stainless steel, RT	2-Tangent	0	0.39	–	–	–	–
6	Contreras et al. [15]	Ferritic-pearlite AE460, [− 60 °C, − 50 °C]	Offset 50 µm t_0/10	207	0.268	269	0.051	–	–
7	Matocha et al. [29]	Carbon steel 22 K and heat treatments, RT	Offset 100 µm t_0/5	0	0.31	–	–	–	–
8	Garcia et al. [26]	Wide variety of steels and one Al alloy	Offset 50 µm t_0/10	0	0.346	–	–	0	0.277
			2-Tangent	0	0.442	268.8	0.065	–	–
			CWA	0	0.476	268.7	0.129	–	–
9	Rodriguez et al. [9]	Wide range of polymers	First max. load–deflection curve	− 0.186	0.12	–	–	–	–
10	Rodriguez et al. [14]	Various sintered materials	Offset t_0/10	0	0.343	0	0.343	–	–
11	Bruchhausen et al. [19]	P-92 Specimen	Offset t_0/10	10.7	0.288	–	–	–	–
			2-Secant	− 34.9	0.405	–	–	–	–
			CWA	28.8	0.382	− 27.04	0.326	− 11.8	0.093
12	Altstadt et al. [30]	T91 steels, RT and 300 °C	2-Secant	0	0.44–0.60	–	–	–	–
13	Janca et al. [31]	Various steels and Al alloys	$F_{e1.5}$	0	0.51	–	–	–	–
14	Simonovski et al. [8]	Grade 91 ferritic steel, RT	CWA	0	0.442	–	–	–	–
			2-Secants	0	0.476	–	–	–	–
			Offset t_0/10	0	0.346	–	–	–	–
15	Moreno [32]	Various Al alloys and steels, RT	(t_0/100, t_0/10, 2-tangents, 2-secant)	0	0.23–0.98	–	–	–	–
16	Peng et al. [33]	316L stainless steel, RT	2-Tangents	25.71	0.69	− 63.97	0.13	–	-
			CWA	50.42	0.77	–	–	–	–
			Offset t_0/10	54.92	0.49	–	–	–	–
			Offset t_0/100	80.02	0.78	–	–	–	–
17	Holmstrom et al. [34]	Various steel alloys [RT, 650 °C]	N.A	–	–	0	0.279	0	0.179

followed to define the yield strength for steels from uniaxial tensile test data. Here, rather offsetting at 0.2% strain, a parallel line to draw at $t_0/10$ displacement with reference of the initial linear elastic slope. Yield load P_y is identified at intersecting point of offset line to the L–D curve as shown in Fig. 11.

Whereas, in the two-tangent method, as shown in Fig. 11, two-tangent lines are drawn from the elastic and plastic bending curves, and the yield load P_y [11] relates to the intersection point of the tangent lines. Moreover, as per CEN CWA 15627:2007 [5] approach, P_y is regarded at the intersection point of L–D curve and vertical line drawn down from the intersection of two-tangent lines.

Mao and Takashi [11] investigated TEM (HT-60) disks and proposed a linear relationship to determine the strengths as a function of applied force and initial specimen thickness as mentioned in Eqs. (5) and (7).

Later Ruan et al. [27] performed SP testing at the variable temperature of 80, 133, 173, and 293 K over the tempered martensitic steel EUROFER97 specimens and concluded that Eqs. (5), (6) driven strength parameters are highly dependent on the temperature as shown in Figs. 12 and 13. The results appear that the yield strength estimation P_y/t_0^2 is highly temperature sensitive below 200 K.

Garcia et al. [26] performed SPT on 16 different material grades of structural steel to stainless steel metal alloys, to scrutinize the best-fit approach for the yield and ultimate strengths estimation. We reference of such a study, the author proposed the distinct empirical correlation factors. Later, Bruchhausen et al. [19] optimized these factors.

Janca et al. [31] attempted to improve the linear correlation Eq. (5), with the aim to make it universally viable for yield strength estimation. Author such correlation as a function of $P_{y1.5}$, as per Eq. (8) which is claimed the superior approach than CWA method. Such $P_{y1.5}$ force is denoted over the L–D curve, where the area under the

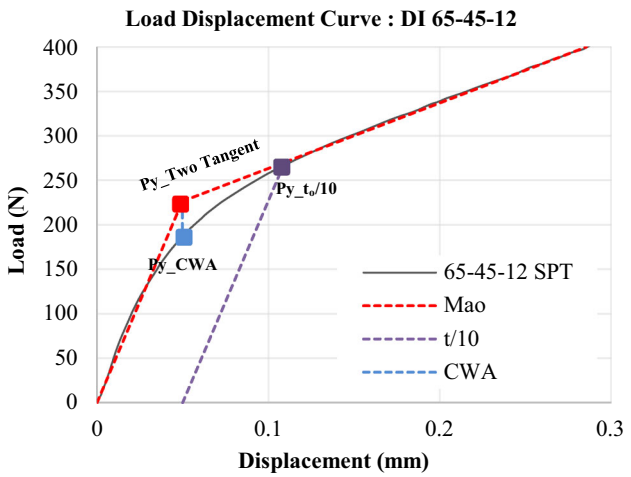

Fig. 11 Determination of P_y by various methods at room temperature

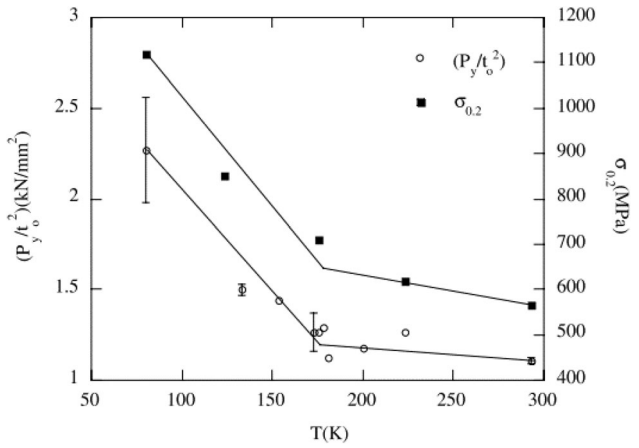

Fig. 12 Temperature dependence of P_y/t_0^2 and of $\sigma_{0.2}$ [27]

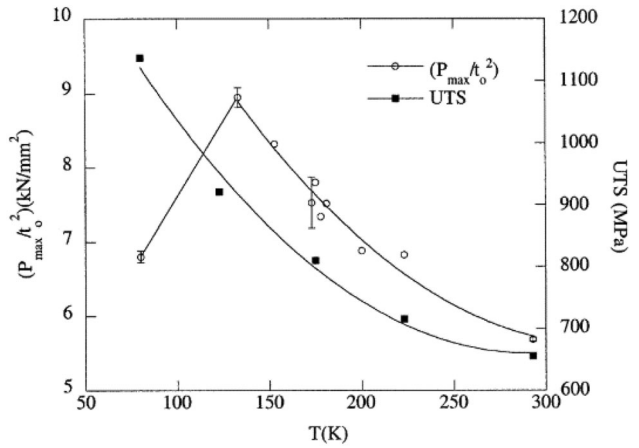

Fig. 13 Temperature dependence of P_{max}/t_0^2 and of UTS [27]

curve is 1.5 times greater than the complimentary area above the curve.

$$\sigma_y = \alpha_1 + \frac{\alpha_2 P_{y1.5}}{t_0^2} \tag{8}$$

Calaf-Chica et al. [36] found that yield strength estimation does not only rely on elastic–plastic transition load obtained with the $t/10$ offset method but also on the minimum slope ($Slope_{min}$) during the membrane stretching region (strain hardening region) of the L–D curve by following Eq. (9), as an attempt to optimize $t/10$ offset method.

$$\sigma_y = \frac{\alpha_2' P_y}{t_0^2} + \frac{\alpha_1' Slope_{min}}{t_0} \tag{9}$$

where α_i' = co-efficient obtained by regression analysis.

Eventually, some of the researchers have also attempted to establish the non-linear correlation Like, Eskner et al. [37], Fleury et al. [20] analyzed the elastic deformation using classical plate bend theory, and found a good agreement between SPT biaxial results with uniaxial tensile data.

$$\sigma_y = \frac{3P_y(1+v)}{2\pi t_0^2}\ln\frac{R}{r} \tag{10}$$

, where P_y = the small punch elastic–plastic load, t_0 = the original thickness, R = the radius of the lower die bore, v = Poisson's ratio, and r = the small punch equivalent contact radius.

Calaf-Chica et al. [38] studied the deviation in yield and ultimate strength estimation in absence of material isotropy and the Bauschinger effect. He observed that in absence of isotropy, the co-efficient of yield strength correlation becomes invalidated.

Isselin et al. [39] have proposed a unique elastic energy compliant approach by correlating it with force to yield strength. The authors stretched the specimen until maximum force to gain extreme plasticity and subsequently unloaded it at the same rate. The area under the L–D curve measured which was observed while reverse deflection until elasticity and defined the elastic energy E_{el} as a function of stress using Eq. (11):

$$E_{el} = \sigma_y^2 \frac{2[1-v^2]R^2h}{3E\pi[1+v^2]} \tag{11}$$

where E = elastic modulus, v = Poisson ratio, and R = radius of an aperture of the lower die. E_{el} = determined experimentally using the load/unload method.

Modulus of Elasticity (E)

The initial slope ($Slope_{ini}$) of L–D curve per Fig. 9, plotted using $t_0/10$ offset method defines Young's modulus of elasticity (E). It can be established as proposed by Cuesta et al. [40]:

$$E = \lambda\left(\frac{Slope_{ini}}{t_0}\right) \tag{12}$$

, where λ = the co-efficient for elastic modulus.

Vorlicek et al. [41] attempted to characterize the mechanical properties for the low-alloy ferritic steel and demonstrated the analytical formulation for E, as a function of various SPT parameters per Eq. 13. However, here, it was assumed that the contact radius remains constant throughout the disk's elastic deformation whereas the contacts are frictionless. As a result, such an assumption leads to underestimation.

$$E = \left(\frac{P_y}{\pi\delta t_0}\right)\left[1.2(1+v)\ln\left(\frac{R}{r}\right) + 0.75R^2\left(1-v^2\right)/t_0^2\right] \tag{13}$$

, where t_0 = initial specimen thickness, δ = specimen displacement, P_y = Yield force, R = the radius of the supporting specimen jig, r = the contact radius, and v = Poisson's ratio.

Chica et al. [18] studied the sensitivity of $Slope_{ini}$ for unloading/loading (UL) cycles and proposed the slope determination with reference of unloading cycle because it exhibits the pure elastic behavior and independent of Poisson's ratio influence. The author proposed the empirical correlation as mentioned in Eq. (14) at the fixed punch displacement at 0.1 mm for UL cycle. He found a good linear agreement (R^2 = 0.9999) using the correlation factor of $\lambda_{UL\_0.1} = 14.84\,mm^{-1}$.

$$E = \lambda_{UL_{0.1}} \cdot Slope_{UL_{0.1}} \tag{14}$$

Nowadays, commercial Finite Element Analysis (FEA) simulation tools are advanced greatly to match the experimental level of accuracy. FE simulation compliments to bring greater insight regarding specimen's structural behavior transformation under the various stages of loading. These imperatives have attracted the attention of researchers to extend the work in the domain of the SP test technique. Recently I. Simonovski et al. [8] used curved specimens extracted from nuclear fuel cladding tubes to correlate the variation in L–D as well as stress–strain behavior with flat specimen under the change of friction between punch and specimen.

Small Punch Test Simulation

As discussed so far, the diverse opinions realized among the researchers to accord the most appropriate SPT empirical correlations which universally comply for the larger group of materials mechanical characterization. The ductile iron material is widely used for general-purpose mechanical product manufacturing which undergoes the high-pressure rating; due to its easy availability and economical raw material cost. Hereby, it is attempted to investigate the SP test methodology and its empirical correlations for the ductile iron, 65-45-12 characterization. This investigation is accomplished through an FEA simulation-driven approach. The ductile iron, 65-45-12 material's uniaxial tensile data are compared with FE simulated SPT L–D response and comparative results are discussed further.

FE Simulation Setup

Hereby, the ANSYS Mechanical Enterprise R19.2 FE [42] FE simulation tool is utilized to conduct the virtual SPT simulations for various boundary conditions. As shown in Figs. 4 and 14, FEA geometries specification is set as per CWA [5]. A flat specimen of size ϕ8 mm × 0.5 mm is considered. The entire assembly is 360° symmetric so it is idealized using axisymmetric behavior and meshed using PLANE183 higher order 2D, 8-node quadrilateral element.

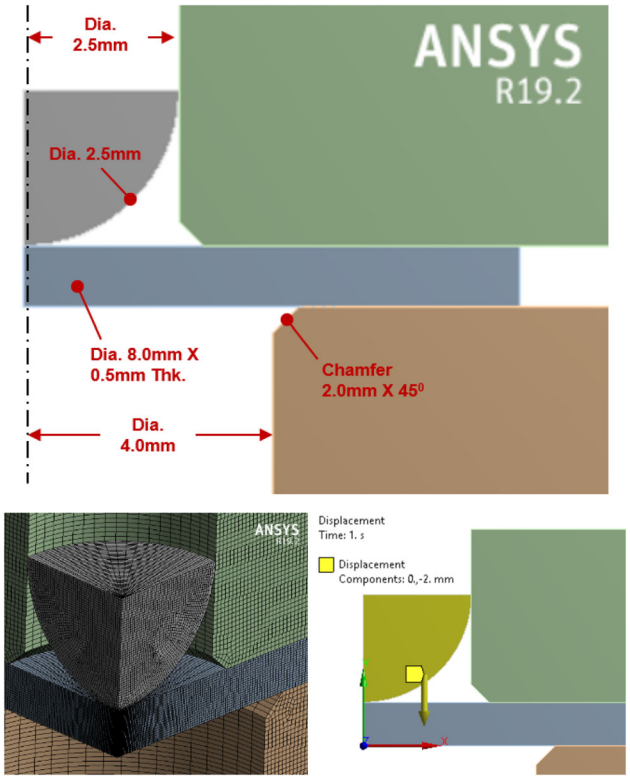

Fig. 14 FEA simulation setup

The specimen is firmly clamped between upper and lower dies and indenter ball punch exerting the force over specimen to displace it.

All the geometries except specimen are defined as a rigid body to capture the inherent specimen stiffness whereas, the specimen's 65-45-12 ductile iron defined using a "multilinear isotropic hardening" material model to capture the isotropic elastic–plastic characteristic and material non-linearity. The true elastic–plastic stress–strain characteristic points are fed as engineering data to follow during the numerical solution convergence.

FEA Methodology Benchmarking

The researchers [19, 20, 26, 43] has typically employed the ABAQUS numerical analysis tool whereas, in this study, ANSYS Mechanical Enterprise 2020 R2 FE [42] tool is explored so it's being essential to benchmark the FEA simulation methodology and computation accuracy with the researchers' simulation and experimental results. For this purpose, the FE simulation boundary conditions are replicated here to conduct ANSYS simulation with reference of the published data by Bruchhausen et al. [19].

Figure 15, shows G91 specimen deformation, extracted from ANSYS FE simulation. The extracted load–displacement relationship is compared with SPT experimental and ABAQUS simulation data in Fig. 16. It is observed the

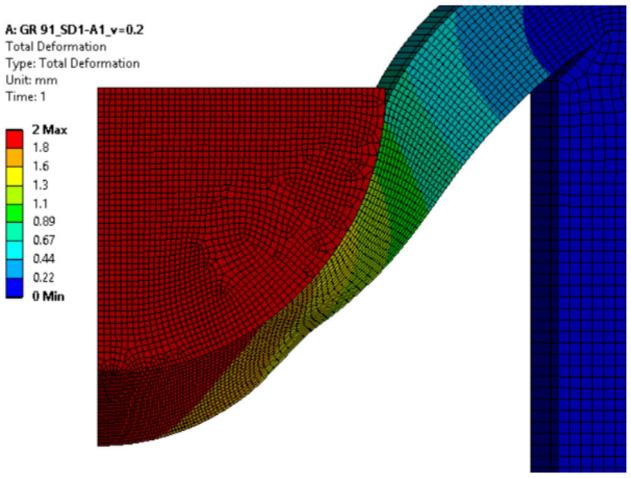

Fig. 15 G91 Steel ANSYS FEM results with $\mu = 0.2$

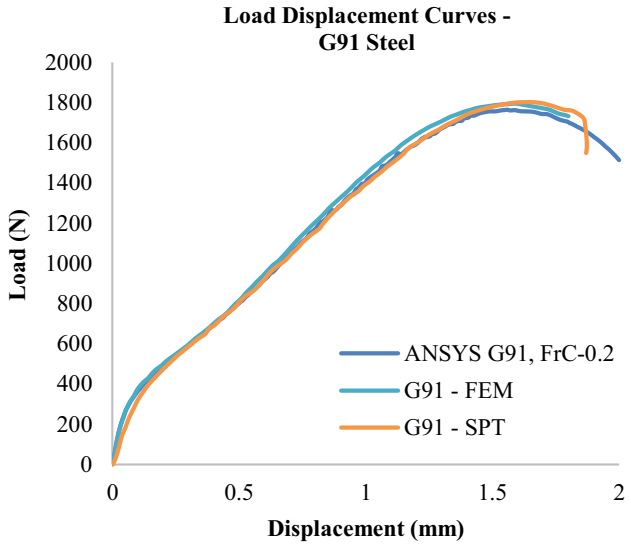

Fig. 16 G91 Steel FEM and SPT [19] load–displacement results benchmarking with ANSYS FEM, $\mu = 0.2$

close match among all of the three L–D results. Such agreement endorses the reliability of ANSYS simulation methodology and computational accuracy for the potential tool to carry over SPT research, as an alternate of experimental testing.

Comparison of Ductile Iron Characterization

Our interest in this study is to verify the strength characterization viability for aged ductile iron 65-45-12 specimen, using the linear Eqs. (5) to (7) and corresponding factors published in the pieces of literature [19, 26] as tabulated in Tables 3 and 4. The FEA simulation-based approach is continued to simulate the SP test parameters.

The material properties of ductile iron, 65-45-12 are defined with reference of Table 2, which are uniaxial

Table 2 Ductile iron, 65-45-12 mechanical properties utilized for FEA simulation

Material	E (GPa)	Poisson's ratio	σ_y (MPa)	σ_u (MPa)
DI, 65-45-12	170	0.275	281	610

Where σ_y = at 0.2% offset and strain hardening co-efficient, n = 7.9

tensile test data, performed over the material extracted from the in-service component.

FEA simulation is performed by considering the 0.2 frictional co-efficient to imitate the SP test boundary conditions as mentioned in the literature [19, 26]. Figure 17 shows the ductile iron SP test L–D response until the rupture phase. Whereas, Fig. 18 shows the subsequent yield force estimation using the (1) 2 tangent method, (2) CWA approach, and (3) $t/10$ offset method.

As tabulated in Table 3, Garcia et al. [26] and Bruchhausen et al. [19] proposed the universal factors for material strength characterization using linear equation and yield load estimated through graphical methods. The yield strength compliance of the SP test with uniaxial data are plotted over Fig. 19, to compare them with yield strength estimation for ductile iron.

Similarly, Table 4 describes initially defined ultimate strength correlation factors by Garcia et al. [26] and subsequently optimized further by Bruchhausen et al. [19]. The ductile iron material's ultimate strengths are estimated with reference of maximum load extracted from Fig. 17, L–D curve and linear Eqs. (6) and (7) with the integration of optimized factors of Bruchhausen et al. [19]. The ductile iron uniaxial and SPT data are compared in Fig. 20.

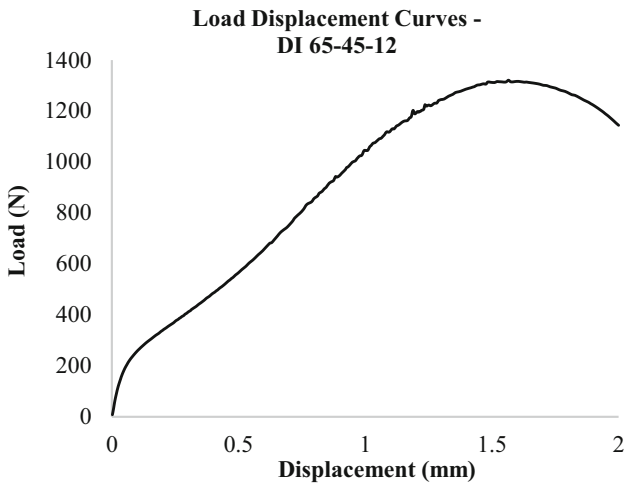

Fig. 17 65-45-12 ductile iron FEM load–displacement results $\mu = 0.2$

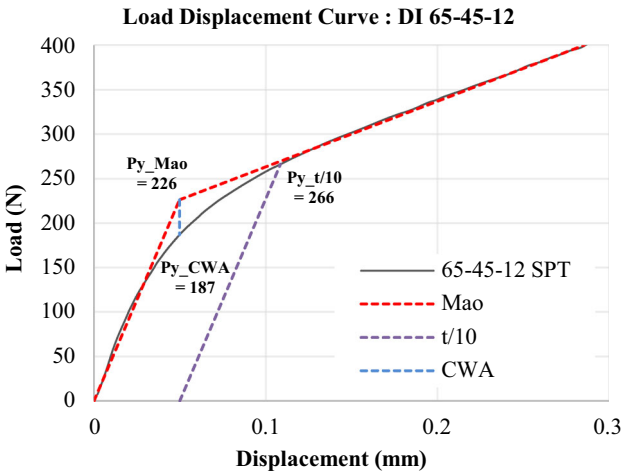

Fig. 18 P_y estimation using various approaches for 65-45-12 Ductile Iron, $\mu = 0.2$

Table 3 Factors proposed by literature for yield strength estimation

Approach	Factor	Garcia et al. [26]	Bruchhausen et al. [19]
CWA	α_1	0	28.8
	α_2	0.476	0.382
Two-tangent	α_1	0	− 34.9
	α_2	0.442	0.405
$t/10$ offset	α_1	0	10.7
	α_2	0.346	0.288

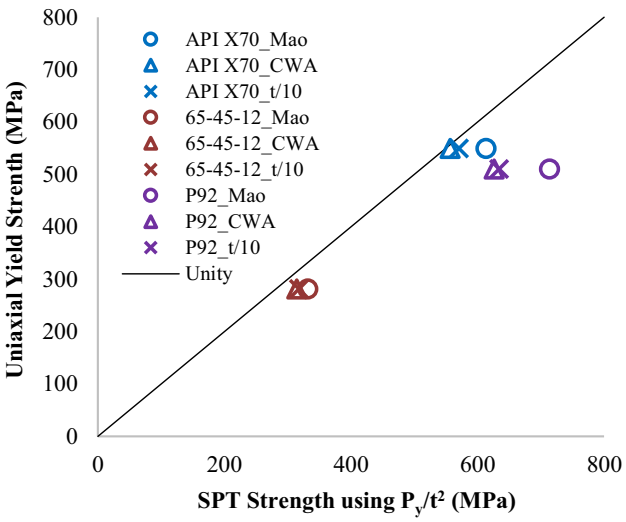

Fig. 19 Uniaxial versus SPT Yield strength estimation using various approaches, API X70 [26], P92 [19]

Results and Discussion

It is observed with reference of Fig. 19 comparative data that the yield strength estimation for all the materials, using CWA [5] and $t/10$ offset methods are closely matching. But

Table 4 Factors proposed by literature for ultimate strength estimation

Factor	Garcia et al. [26]	Bruchhausen et al. [19]
β_1	0	− 27.04
β_2	0.277	0.326
β_1'	268.81	− 11.86
β_2'	0.065	0.093

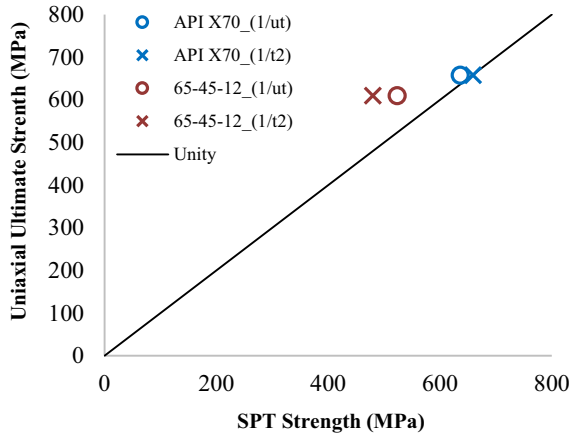

Fig. 20 Uniaxial versus SPT Ultimate strength estimation using various approaches, API X70 [26]

still, there are gaps to correlate the SPT estimated strengths with uniaxial data, because all of them deviate from the unity line.

Moreover, it is also noticed from Fig. 20 data, that ultimate strength estimation is reliable using Eq. (6) for API X70 but it is not true for ductile iron. The proposed factors are not competent to determine the ultimate strength accurately for ductile iron, using any of the linear equations.

Overall, the relevance of proposed optimized factors for ductile iron material is subjective and such inconsistency may be primarily due to variation in materials elastic and plastic stiffness along with its bulk modulus.

Summary

Overall, it is perceived the potential of SP testing for in-service components' mechanical characterization, rather to rely on traditional universal tensile testing. However, there are certain challenges, which need to be addressed to make this technique more robust, reliable, and universal to comply for the wider class and nature of materials. As we studied earlier, one of the greatest challenges is for appropriate post-processing of SPT L–D data to establish the uniaxial stress–strain constitutive relationship. Many graphical and analytical methods exist in public but their reliability is highly subjective and distinct to specimen's material along with the test boundary conditions. The analytical linear correlation factors diverge significantly for different classes of materials. Some researchers [34, 39, 44] have also formulated non-linear equations with the assumption of plasticity theory using an inverse predictive method for stress–strain behavior. These analytical formulations are complicated to interpret and adopt too.

Moreover, the SP test L–D characteristic is sensitive to the testing parameters like indenter ball punch to specimen size ratio, specimen thickness, and shape.

As we realized the scattered results for ductile iron, 65-45-12 material strength characterization using the published factors and characterization methods, prompts the great scope of improvement for the SP testing methodology and guideline to post-process the results for accurate mechanical characterization for the universal class of materials. It is pretty much challenging to get a micro-level insight into specimen behavior during physical experimental SP testing. Here, it crucial to exploit the virtues of FEA simulation techniques to overcome the known issues.

References

1. M.P. Manahan, A.S. Argon, O.K. Harling, The development of a miniaturized disk bend test for the determination of postirradiation mechanical properties. J. Nucl. Mater. **104**, 1545–1550 (1981). https://doi.org/10.1016/0022-3115(82)90820-0
2. J. Kameda, O. Buck, Evaluation of the ductile-to-brittle transition temperature shift due to temper embrittlement and neutron irradiation by means of a small-punch test. Mater. Sci. Eng. **83**, 29–38 (1986). https://doi.org/10.1016/0025-5416(86)90171-0
3. J.M. Baik, J. Kameda, O. Buck, Small punch test evaluation of intergranular embrittlement of an alloy steel. Scr. Metall. **17**, 1443–1447 (1983). https://doi.org/10.1016/0036-9748(83)90373-3
4. G.E. Lucas, The development of small specimen mechanical test techniques. J. Nucl. Mater. **117**, 327–339 (1983). https://doi.org/10.1016/0022-3115(83)90041-7
5. CEN Workshop Agreement, Small Punch Test Method for Metallic Materials, CWA 15627:2007 (2007)
6. T. Misawa, T. Adachi, M. Saito, Y. Hamaguchi, Small punch tests for evaluating ductile-brittle transition behavior of irradiated ferritic steels. J. Nucl. Mater. **150**, 194–202 (1987). https://doi.org/10.1016/0022-3115(87)90075-4
7. T. Misawa, H. Sugawara, R. Miura, Y. Hamaguchi, Small specimen fracture toughness tests of HT-9 steel irradiated with protons. J. Nucl. Mater. **133–134**, 313–316 (1985). https://doi.org/10.1016/0022-3115(85)90158-8
8. I. Simonovski, S. Holmström, M. Bruchhausen, Small punch tensile testing of curved specimens: Finite element analysis and experiment. Int. J. Mech. Sci. **120**, 204–213 (2017). https://doi.org/10.1016/j.ijmecsci.2016.11.029
9. C. Rodríguez, I.I. Cuesta, M.L.L. Maspoch, F.J. Belzunce, Application of the miniature small punch test for the mechanical characterization of polymer materials. Theor. Appl. Fract. Mech. **86**, 78–83 (2016). https://doi.org/10.1016/j.tafmec.2016.10.001

10. D. Sánchez-Ávila, R. Barea, E. Martínez, J.R. Blasco, L. Portolés, F. Carreño, Determination of the instantaneous strain rate during small punch testing of 316 L stainless steel. Int. J. Mech. Sci. **149**, 93–100 (2018). https://doi.org/10.1016/j.ijmecsci.2018.09.042
11. X. Mao, H. Takahashi, Development of a further-miniaturized specimen of 3 mm diameter for tem disk (ø3 mm) small punch tests. J. Nucl. Mater. **150**, 42–52 (1987). https://doi.org/10.1016/0022-3115(87)90092-4
12. X. Mao, T. Shoji, H. Takahashi, Characterization of fracture behavior in small punch test by combined recrystallization-etch method and rigid plastic analysis. J. Test. Eval. **15**, 30–37 (1987). https://doi.org/10.1520/JTE11549J
13. H. Takahashi, T. Shoji, X. Mao, Recommended practice for small punch (SP) testing of metallic materials, JAERI-M–88-172 (1988)
14. C. Rodríguez, M. Fernández, J.G. Cabezas, T.E. García, F.J. Belzunce, The use of the small punch test to solve practical engineering problems. Theor. Appl. Fract. Mech. **86**, 109–116 (2016). https://doi.org/10.1016/j.tafmec.2016.08.021
15. M.A. Contreras, C. Rodríguez, F.J. Belzunce, C. Betegón, Use of the small punch test to determine the ductile-to-brittle transition temperature of structural steels. Fatigue Fract. Eng. Mater. Struct. **31**, 727–737 (2008). https://doi.org/10.1111/j.1460-2695.2008.01259.x
16. J. D. Parker, A. McMinn, and J. Foulds, Material sampling for the assessment of component integrity, PVP ASME 171, 223-230, (1989)
17. P. Roberts, I. Dane, Scoop Sampling for Small Punch Test Method, Rolls-Royce Naval Marine. Present. to CEN/WS21-UNI, Milan (2004)
18. J.C. Chica, P.M. Bravo Díez, M. Preciado Calzada, Improved correlation for elastic modulus prediction of metallic materials in the small punch test. Int. J. Mech. Sci. **134**, 112–122 (2017). https://doi.org/10.1016/j.ijmecsci.2017.10.006
19. M. Bruchhausen, S. Holmström, I. Simonovski, T. Austin, J.M. Lapetite, S. Ripplinger, F. de Haan, Recent developments in small punch testing: tensile properties and DBTT. Theor. Appl. Fract. Mech. **86**, 2–10 (2016). https://doi.org/10.1016/j.tafmec.2016.09.012
20. E. Fleury, J.S. Ha, Small punch tests to estimate the mechanical properties of steels for steam power plant: I. Mechanical strength. Int. J. Press. Vessels Pip. **75**, 707–713 (1998). https://doi.org/10.1016/S0308-0161(98)00075-1
21. J. Kameda, X. Mao, Small-punch and TEM-disc testing techniques and their application to characterization of radiation damage. J. Mater. Sci. **27**, 983–989 (1992). https://doi.org/10.1007/BF01197651
22. W.D. Pilkey, *Formula for Stress, Strain, and Structural Matrices* (Wiley Interscience, New York, 1994)
23. D. Drucker, Conventional and unconventional plastic response and representation. Appl. Mech. Rev. **41**, 155–167 (1988). https://doi.org/10.1115/1.3151888
24. N. Wang, Large plastic deformation of a circular sheet caused by punch stretching. J. Appl. Mech. Trans. ASME **37**, 431–440 (1970). https://doi.org/10.1115/1.3408524
25. G.E. Lucas, A. Okada, M. Kiritani, Parametric analysis of the disc bend test. J. Nucl. Mater. **141–143**, 532–535 (1986). https://doi.org/10.1016/S0022-3115(86)80096-4
26. T.E. García, C. Rodríguez, F.J. Belzunce, C. Suárez, Estimation of the mechanical properties of metallic materials by means of the small punch test. J. Alloys Compd. **582**, 708–717 (2014). https://doi.org/10.1016/j.jallcom.2013.08.009
27. Y. Ruan, P. Spätig, M. Victoria, Assessment of mechanical properties of the martensitic steel EUROFER97 by means of punch tests. J. Nucl. Mater. **307–311**, 236–239 (2002). https://doi.org/10.1016/S0022-3115(02)01194-7
28. E.N. Campitelli, P. Spätig, R. Bonadé, W. Hoffelner, M. Victoria, Assessment of the constitutive properties from small ball punch test: experiment and modeling. J. Nucl. Mater. **335**, 366–378 (2004). https://doi.org/10.1016/j.jnucmat.2004.07.052
29. K. Matocha, M. Filip, S. Stejskalova, Determination of critical temperature of brittleness TK0 by small punch tests, in *Proceedings of COMAT2012—Recent Trends In Structural Materials* (2012)
30. E. Altstadt, H.E. Ge, V. Kuksenko, M. Serrano, M. Houska, M. Lasan, M. Bruchhausen, J.-M. Lapetite, Y. Dai, Critical evaluation of the small punch test as a screening procedure for mechanical properties. J. Nucl. Mater. **472**, 186–195 (2016). https://doi.org/10.1016/j.jnucmat.2015.07.029
31. A. Janča, J. Siegl, P. Haušild, Small punch test evaluation methods for material characterisation. J. Nucl. Mater. **481**, 201–213 (2016). https://doi.org/10.1016/j.jnucmat.2016.09.015
32. M.F. Moreno, Effects of thickness specimen on the evaluation of relationship between tensile properties and small punch testing parameters in metallic materials. Mater. Des. **157**, 512–522 (2018). https://doi.org/10.1016/j.matdes.2018.07.065
33. J. Peng, K. Li, Q. Dai, G. Gao, Y. Zhang, W. Cao, Estimation of mechanical strength for pre-strained 316L austenitic stainless steel by small punch test. Vacuum **160**, 37–53 (2019). https://doi.org/10.1016/j.vacuum.2018.11.015
34. S. Holmström, I. Simonovski, D. Baraldi, M. Bruchhausen, E. Altstadt, R. Delville, Developments in the estimation of tensile strength by small punch testing. Theor. Appl. Fract. Mech. **101**, 25–34 (2019). https://doi.org/10.1016/j.tafmec.2019.01.020
35. S. Haroush, E. Priel, D. Moreno, A. Busiba, I. Silverman, A. Turgeman, R. Shneck, Y. Gelbstein, Evaluation of the mechanical properties of SS-316L thin foils by small punch testing and finite element analysis. Mater. Des. **83**, 75–84 (2015). https://doi.org/10.1016/j.matdes.2015.05.049
36. J. Calaf-chica, P. Miguel, B. Díez, M.P. Calzada, Optimization of the t/10 offset correlation method to obtain the yield strength with the small punch test. J. Nucl. Mater. **534**, 152177 (2020). https://doi.org/10.1016/j.jnucmat.2020.152177
37. M. Eskner, R. Sandstrom, Mechanical property evaluation using the small punch test. J. Test. Eval. **32**, 1–8 (2004). https://doi.org/10.1520/JTE11504
38. J. Calaf-Chica, M.S. Palomar, P.M.B. Díez, M.P. Calzada, Deviations in yield and ultimate tensile strength estimation with the small punch test: numerical analysis of pre-straining and Bauschinger effect influence. Mech. Mater. **153**, 103696 (2021). https://doi.org/10.1016/J.MECHMAT.2020.103696
39. J. Isselin, T. Shoji, Yield strength evaluation by small-punch test. J. Test. Eval. **37**, 531–537 (2009). https://doi.org/10.1520/JTE101657
40. I.I. Cuesta, C. Rodríguez, T.E. García, J.M. Alegre, Effect of confinement level on mechanical behaviour using the small punch test. Eng. Fail. Anal. **58**, 206–211 (2015). https://doi.org/10.1016/j.engfailanal.2015.09.008
41. V. Vorlicek, L. Exworthy, P.E. Flewitt, Evaluation of a miniaturized disc test for establishing the mechanical properties of low-alloy ferritic steels. J. Mater. Sci. **30**, 2936–2943 (1995). https://doi.org/10.1007/BF00349666
42. ANSYS Mechanical Enterprise, ANSYS Inc. (2019). https://www.ansys.com/en-in/products/structures/ansys-mechanical
43. I. Simonovski, D. Baraldi, S. Holmström, E. Altstadt, R. Delville, M. Bruchhausen, Determining the ultimate tensile strength of fuel cladding tubes by small punch testing. J. Nucl. Mater. **509**, 620–630 (2018). https://doi.org/10.1016/j.jnucmat.2018.07.041

44. J. Chakrabarty, A theory of stretch forming over hemispherical punch heads. Int. J. Mech. Sci. **12**, 315–325 (1970). https://doi.org/10.1016/0020-7403(70)90085-8